

Estimating the Longitudinal Centre of Flotation of a Vessel in Waves using Acceleration Measurements

Nana O. Abankwa, James Bowker, Steven J. Johnston, Mark Scott, and Simon J. Cox

Abstract—The location of a vessel's centre of flotation during operation at sea plays an important role in the vessel's longitudinal stability. The ability to accurately estimate the location of the centre of flotation improves safety monitoring as it indicates how changes in the distribution of weight affect the vessel. In this study, we propose a novel method for estimating the longitudinal location of a vessel's centre of flotation in waves using acceleration readings taken simultaneously at different locations along the length of the vessel. Specifically, we recorded accelerations of an autonomous surface vehicle (ASV) in a towing tank. The ASV was operated in head and following regular waves, which were kept at a constant wave height of 0.12 m while the wave frequency was increased from 0.5 Hz to 0.8 Hz at increments of 0.1 Hz. The results show that multiple acceleration measurements can be used to correctly determine the centre of flotation of a vessel in waves. In this experiment, the estimated location of the centre of flotation varied as expected based on the longitudinal asymmetry of the ASV and the difference between head and following waves, demonstrating the effectiveness of the proposed method. In addition, the results were validated using the vessel's recorded pitch motion.

Index Terms—Qualisys, accelerometers, centre of rotation, centre of flotation, vessel safety, vessel stability.

I. INTRODUCTION

DURING operation at sea, knowledge of essential vessel parameters such as the location of the centre of flotation, allows operators to objectively make informed decisions regarding vessel stability and safety. Stability is affected by factors including a vessel's weight distribution and the shape of its hull [1]. The continuous redistribution of fuel and water weight during normal operation [2] continuously changes a vessel's trim about its centre of flotation [3]. The centre of flotation is defined as the centre of gravity of a vessel's waterplane area [4].

The interaction of the forces of gravity and buoyancy on a vessel determine its centre of rotation. There have been a number of studies investigating the point about which a vessel rotates due to the resultant forces on it during operation [5], [6]. This location is important for many reasons including its effect on a vessel's capsizing probability [7]. Considering the dynamics of rotational motion, a study [8] found the centre of rotation when a vessel is pitching or rolling to coincide with the dynamical definition of a vessel's metacentre. The dynamical definition of the metacentre has been shown [6] to

coincide with Dupin's [9] and Bougeur's [10], [11] definitions of the metacentre. The use of the metacentre as the centre of rotation of a vessel assumes that the centre of flotation is fixed [8]. This is not true as the submerged area and the centre of this area are constantly changing when a vessel is pitching or rolling. Therefore, in this paper, we will assume the centre of oscillatory movement of a vessel pitching or rolling is at the centre of flotation [5].

Accelerometers have been applied to a wide range of problems including human activity classification [12], structural vibration monitoring [13] and tilt sensing [14]. A previous study [15] proposed a method for estimating the centre of gravity of an aerial vehicle using accelerometers arranged in rings. The chosen approach was validated using a simulation modelling an object subjected to various forces and torques. The proposed method showed the importance of having sufficient angular motion for robust estimation of the location of the centre of gravity. This study also demonstrated that more accelerometers improve the estimation. This approach had the disadvantage of requiring knowledge of the aerial vehicle's moment of inertia, mass, and torque. Another study [16] used an approach also involving accelerometers but not arranged in rings to determine the centre of gravity of a spacecraft. Both methods mentioned identified the need for the precision of all accelerometers used to be very high, and for there to be sufficient angular motion. They were also both based on the five-term acceleration equation for determining the acceleration of a particle in a rotating reference frame [17]. Even though methods have been developed for determining the centre of rotation of spacecrafts and aerial vehicles using accelerometer readings, none have been experimentally applied to a vessel in waves.

Knowledge of significant changes in the centre of flotation's location is important because it informs an operator of safety-related issues such as trapped water on deck, which can be dealt with by opening freeing ports. This knowledge can also be used to improve ship handling [18], [19]. The centre of flotation is important when loading and unloading a vessel because for a load to have no effect on the vessel's trim, it must be added or removed at the centre of flotation [3]. This paper aims to develop a method for applying the five-term acceleration equation to finding the centre of flotation of a vessel in waves. The methodology is tested using acceleration readings at multiple points on an autonomous surface vehicle (ASV) in a towing tank. An optical motion capture system is used to measure the accelerations, and the estimated centre of flotation is validated by comparing the maximum and minimum pitch motions computed using the estimated location of the centre of flotation with maximum and minimum pitch

The authors are in the Faculty of Engineering and the Environment, Bolderwood Innovation Campus, University of Southampton, SO16 7QF, United Kingdom (Corresponding author email: n.abankwa@soton.ac.uk).

Manuscript received - ; revised - ; accepted - . Date of publication - . The associate editor coordinating the review of this paper and approving it for publication was Prof. Danilo Demarchi.

Digital Object Identifier -

motions recorded by the optical motion capture system.

The focus of this paper is on the demonstration of a novel data implementation technique for determining the centre of flotation of a vessel in waves, which is independent of the data's acquisition method. The proposed method is applicable to acceleration measurements whether they are recorded by optical motion capture systems [20], [21], traditional accelerometers [22]–[24] or a global positioning system [25], [26].

II. EXPERIMENTAL SETUP

The data collection process was conducted in the University of Southampton Bolderwood Campus towing tank (Figure 1). The tank is 138 m long, 6 m wide and 3.5 m deep, and has a wavemaker that can model sea states up to 0.7 m significant wave height (Figure 2).



Fig. 1: University of Southampton Bolderwood campus towing tank [27].

The particulars of the free-running vehicle used are given in Table I. The autonomous surface vehicle, which had two submerged foils for propulsion along the towing tank [28], was tested in head and following regular waves, which were kept at a constant wave height of 0.12 m. The wave frequency was increased from 0.5 Hz to 0.8 Hz at increments of 0.1 Hz as summarised in Table II.

TABLE I: Particulars of the Autonomous Surface Vehicle.

| Parameter | Value | Units |
|------------------------|----------|-------|
| Length, L | 2.27 | m |
| Beam, B | 0.30 | m |
| Draft, T | 0.10 | m |
| Displacement, Δ | 52.00 | kg |
| Chord, c | 0.23 | m |
| Span, s | 1.00 | m |
| Foil type | NACA0012 | - |
| Foil arm, a | 0.40 | m |

The ASV was stationed at the carriage 30 m from the wavemaker and progressed towards the wavemaker in head waves before being turned around and tested in following waves. The period for each run varied from 60 to 180 seconds depending on the forward speed of the ASV and the wave

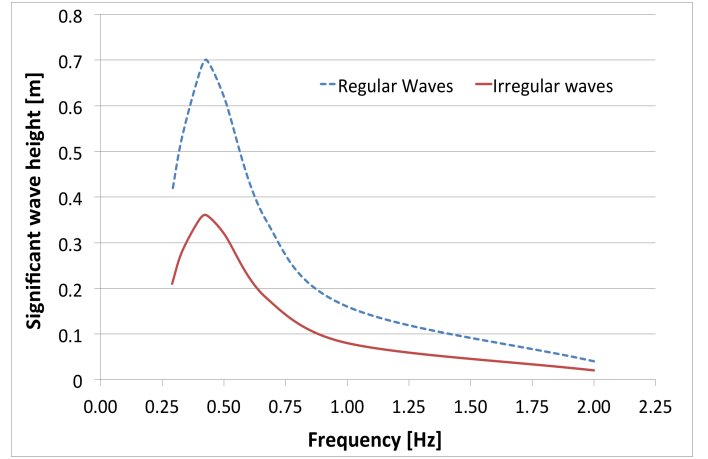


Fig. 2: Wavemaker capability of towing tank [27].

TABLE II: Summary of details of runs.

| Run number | Vessel direction with respect to wavemaker | Wave Amplitude (m) | Wave Frequency (Hz) |
|------------|--|--------------------|---------------------|
| 1 | Towards | 0.06 | 0.50 |
| 2 | Away | 0.06 | 0.50 |
| 3 | Towards | 0.06 | 0.60 |
| 4 | Away | 0.06 | 0.60 |
| 5 | Towards | 0.06 | 0.70 |
| 6 | Away | 0.06 | 0.70 |
| 7 | Towards | 0.06 | 0.80 |
| 8 | Away | 0.06 | 0.80 |

reflection from the opposite end of the tank. During each run, the optical motion capture system (Qualisys) recorded the vessel's pitch and heave displacements and accelerations. The optical motion capture system consisted of eight Oqus 500+ cameras and captured the ASV's motions in six degrees of freedom (DOF) at a rate of 60 Hz. Each camera had a maximum capture distance of 25 m and a 49° horizontal field of vision [29].

As shown in Figure 4, all eight cameras were placed in a row along one side of the towing tank due to practical mounting restrictions. Eight cameras were used to ensure a long coverage volume. This enabled the ASV to remain within the view of the cameras for a sufficient amount of time while it travelled along the length of the towing tank. With the trajectory of the ASV 3.5 m from the cameras, each camera with a horizontal view of 49° covered a length of 3.2 m. Since each unit length was viewed by at least two cameras, the system covered a total length of 12.8 m.

The cameras were daisy-chained and connected to a laptop running the Qualisys Track Manager software (v2.12). This software's graphical user interface (GUI) enables the user to control the cameras' settings, start and stop recording, calibrate the system, and playback recorded runs. A summary of the camera marker settings and video settings used in this setup are presented in Table III.

The Qualisys software computed 3-dimensional (3D) and 6 DOF data from 2-dimensional (2D) marker data. With a

TABLE III: Qualisys Camera Settings.

(a) Marker Settings

| Property | Value |
|------------------|----------------|
| Capture rate | 60 Hz |
| Exposure time | 0.0005 s |
| Marker threshold | 15 % |
| Marker type | Passive |
| Sensor mode | 4 MP at 179 Hz |

(b) Video Settings

| Property | Value |
|---------------|----------------|
| Capture rate | 13 Hz |
| Exposure time | 0.076903 s |
| Flash time | 0.002 s |
| Gain | 4 |
| Sensor mode | 4 MP at 179 Hz |

measuring volume of 1 x 5 x 10 m, the system provides angular accuracy of 0.05 degrees and spatial accuracy of 0.25 mm [30]. In order for the software to properly compute 3D data from 2D camera images, a wand calibration technique was used to determine the orientations of the cameras. This method used 2 objects to calibrate the optical motion capture system. These objects were an L-shaped structure with 4 markers and a wand with 2 markers. The wand was moved through as many different positions and orientations as possible through the volume the ASV was expected to operate in, with the cameras recording at 100 Hz. The L-frame was fixed throughout the experiment to determine the reference frame. Once the calibration was completed, when tracking markers, the system determined the 3D location of a marker $[X_{world} \ Y_{world} \ Z_{world} \ 1]^T$ from the 2D camera image $[x_{camera} \ y_{camera} \ 1]^T$ using the pin-hole camera model



Fig. 4: Arrangement of cameras in towing tank.

[31]–[33] represented in Equation 1.

$$\begin{bmatrix} x_{camera} \\ y_{camera} \\ 1 \end{bmatrix} = K \times [R \ | \ t] \times \begin{bmatrix} X_{world} \\ Y_{world} \\ Z_{world} \\ 1 \end{bmatrix} \quad (1)$$

where

K , is a 3 x 3 intrinsic camera property matrix,
 R , is a 3 x 3 extrinsic rotation matrix,
 t , is a 3 x 1 extrinsic translation matrix, and
 \times , indicates the cross product of 2 matrices.

The optical motion capture system's reference frame is shown in Figure 3 with the positive x-direction being towards the wavemaker, the positive y-direction being towards the mounted cameras, and the positive z-direction being upwards. Figure 3 also shows the location of the five markers which

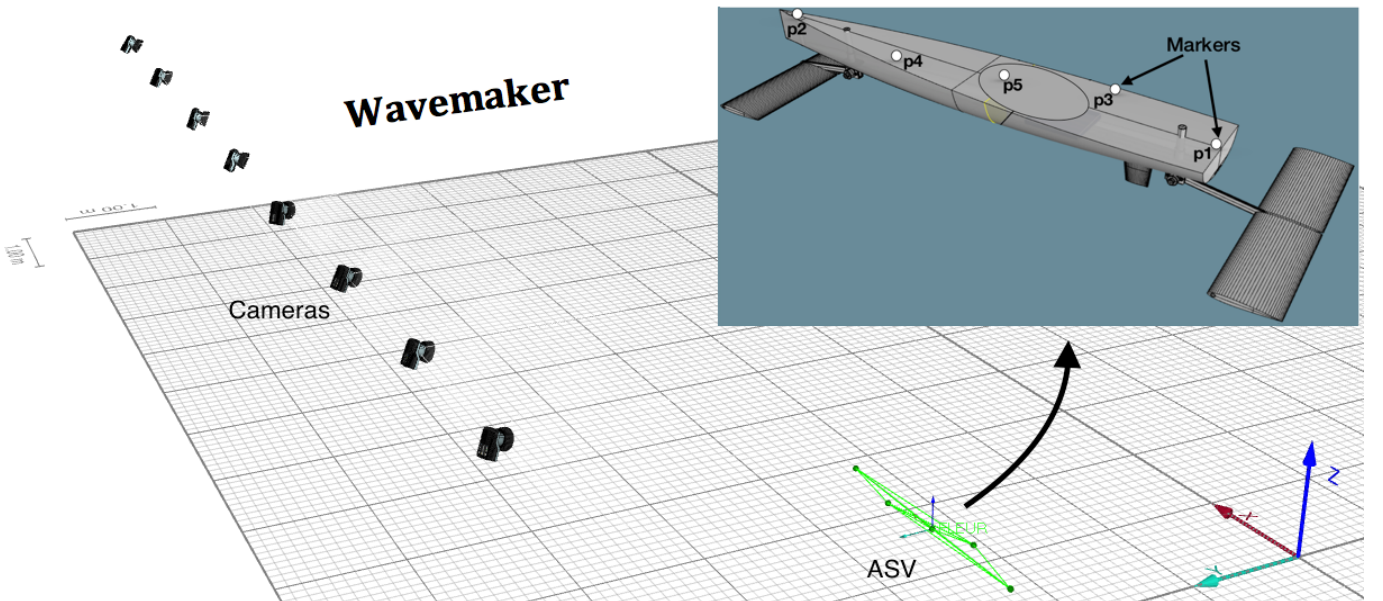


Fig. 3: Experimental setup showing the 8 mounted cameras, the location of the wavemaker, and the position of the markers on the ASV.

indicate the locations of the acceleration readings. The markers were placed asymmetrically to enable the optical motion capture system to better distinguish between them, and for unique definition of the ASV's orientation. Two of the markers were placed at each end of the ASV (the longitudinal limits of the location of the centre of rotation). This ensured that there was at least one marker on either side of the centre of flotation. Five markers were used in total as four markers are recommended for redundancy, with at least three required to define the ASV as a rigid body [34].

III. UNDERLYING THEORY

The method for estimating the centre of rotation of a vessel in waves using accelerometers is based on the concept of the acceleration of a point in a rotating coordinate system [35], [36]. Figure 5 shows the general case of a rotating coordinate system centred at point O (a vessel, $X^bY^bZ^b$) and a fixed coordinate system (flat non-rotating Earth, XYZ) being related by translation and rotation.

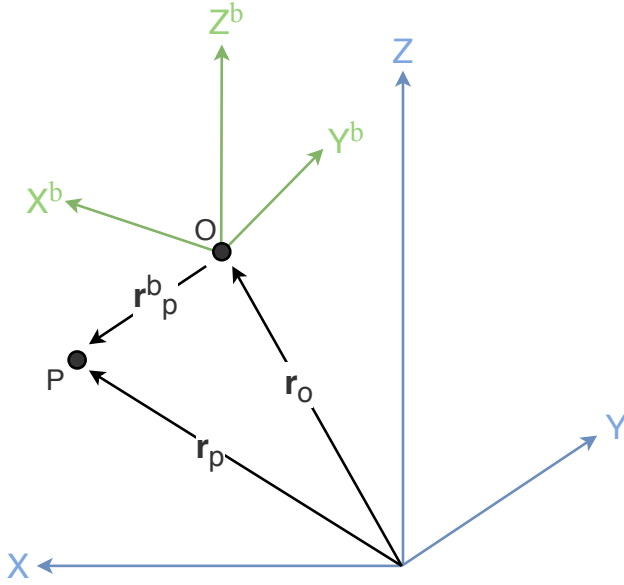


Fig. 5: A translating, rotating reference frame (a vessel, $X^bY^bZ^b$) in a fixed reference frame (flat non-rotating Earth, XYZ)

The measurements of an accelerometer at point P can be calculated as:

$$\mathbf{a}_P = \mathbf{a}_O + (\dot{\omega} \times \mathbf{r}_P^b) + \omega \times (\omega \times \mathbf{r}_P^b) + (2\omega \times \mathbf{v}_P^b) + \mathbf{a}_P^b - \mathbf{F}_{\text{ext}} \quad (2)$$

where

- \mathbf{a}_P , is the inertial acceleration of point P,
- \mathbf{a}_O , is the inertial acceleration of point O,
- ω , is the angular velocity of the body,
- $\dot{\omega}$, is the angular acceleration of the body,
- \mathbf{r}_P^b , is the displacement from point O to point P,
- \mathbf{a}_P^b , is the acceleration of point P relative to point O,
- \mathbf{v}_P^b , is the velocity of point P relative to point O,
- \times , indicates the cross product of 2 vectors, and

\mathbf{F}_{ext} , is any additional acceleration due to external forces such as gravity.

Assuming point O and point P do not move within the body, there is no relative acceleration and no relative velocity between point O and point P in the translating, rotating reference frame ($\mathbf{a}_P^b = 0$ and $\mathbf{v}_P^b = 0$). Equation 2 is reduced to

$$\mathbf{a}_P = \mathbf{a}_O + (\dot{\omega} \times \mathbf{r}_P^b) + \omega \times (\omega \times \mathbf{r}_P^b) - \mathbf{F}_{\text{ext}} \quad (3)$$

Equation 3 is simplified by replacing the cross product operation with the equivalent skew-symmetric matrices [37].

$$\mathbf{a}_P = \mathbf{a}_O + (\mathbf{H}_1 + \mathbf{H}_2)\mathbf{r}_P^b - \mathbf{F}_{\text{ext}} \quad (4)$$

where

$$\mathbf{H}_1 = \begin{bmatrix} 0 & -\dot{\omega}_z & \dot{\omega}_y \\ \dot{\omega}_z & 0 & -\dot{\omega}_x \\ -\dot{\omega}_y & \dot{\omega}_x & 0 \end{bmatrix}$$

$$\mathbf{H}_2 = \begin{bmatrix} -(\omega_y^2 + \omega_z^2) & \omega_x\omega_y & \omega_x\omega_z \\ \omega_x\omega_y & -(\omega_x^2 + \omega_z^2) & \omega_y\omega_z \\ \omega_x\omega_z & \omega_y\omega_z & -(\omega_x^2 + \omega_y^2) \end{bmatrix}$$

If all accelerations due to external forces on a rotating, translating body are known, the inertial acceleration at point P on the body can be determined using Equation 4 if the acceleration at point O on the body, the displacement between the two points, the angular acceleration and the angular velocity of the body are known.

In this experimental setup, \mathbf{H}_1 and \mathbf{H}_2 are common to all of the marker locations since markers 1, 2, 3, 4 and 5 are all on the same body. Using Equation 4 and only accelerometer information from a single marker to estimate the location of the centre of rotation is impossible as this requires knowledge of all external forces, the acceleration at the centre of rotation, the angular velocity, and the angular acceleration measurements used in calculating \mathbf{H}_1 and \mathbf{H}_2 .

In order to simplify the problem and eliminate the requirement of knowing all the external forces on the ASV, the acceleration measurements at points 2, 3, 4, and 5 are subtracted from the acceleration measurements at point 1 as depicted in Equation 5.

$$\begin{aligned} \mathbf{a}_1 - \mathbf{a}_i &= (\mathbf{H}_1 + \mathbf{H}_2)(\mathbf{r}_1^b - \mathbf{r}_i^b) \\ \mathbf{a}_1 - \mathbf{a}_i &= \mathbf{H}(\mathbf{r}_1^b - \mathbf{r}_i^b) \quad i = 2, 3, 4, 5 \end{aligned} \quad (5)$$

From Equation 5, \mathbf{H} can be determined since the acceleration measurements and positions of the 5 markers are known. Equation 5 is solved using an ordinary least squares regression [38] without an intercept when rewritten as

$$\begin{aligned} \mathbf{r}_1^b - \mathbf{r}_i^b &= \mathbf{H}^{-1}(\mathbf{a}_1 - \mathbf{a}_i) \\ \begin{bmatrix} x_1^b - x_i^b \\ y_1^b - y_i^b \\ z_1^b - z_i^b \end{bmatrix} &= \begin{bmatrix} h_{11}^{-1} & h_{12}^{-1} & h_{13}^{-1} \\ h_{21}^{-1} & h_{22}^{-1} & h_{23}^{-1} \\ h_{31}^{-1} & h_{32}^{-1} & h_{33}^{-1} \end{bmatrix} \begin{bmatrix} \ddot{x}_1 - \ddot{x}_i \\ \ddot{y}_1 - \ddot{y}_i \\ \ddot{z}_1 - \ddot{z}_i \end{bmatrix} \end{aligned} \quad (6)$$

Relative position = Coefficient \times Relative acceleration

An alternative approach to solving for the location of the centre of flotation using accelerometer readings is to reformulate the regression problem as a linear state-space model, solved using Kalman filters [39], [40].

Equation 6 assumes that the x, y, and z components of the relative acceleration need to interact with each other to produce significant relationships with the x, y, and z components of the relative position. However this is not true because there was minimal roll motion so the problem will be considered as a set of simple regression equations.

$$\begin{aligned}
 x_1^b - x_i^b &= h_{11}^{-1} \cdot (\ddot{x}_1 - \ddot{x}_i) \\
 y_1^b - y_i^b &= h_{12}^{-1} \cdot (\ddot{y}_1 - \ddot{y}_i) \\
 z_1^b - z_i^b &= h_{13}^{-1} \cdot (\ddot{z}_1 - \ddot{z}_i) \\
 \\
 y_1^b - y_i^b &= h_{21}^{-1} \cdot (\ddot{x}_1 - \ddot{x}_i) \\
 y_1^b - y_i^b &= h_{22}^{-1} \cdot (\ddot{y}_1 - \ddot{y}_i) \\
 y_1^b - y_i^b &= h_{23}^{-1} \cdot (\ddot{z}_1 - \ddot{z}_i) \\
 \\
 z_1^b - z_i^b &= h_{31}^{-1} \cdot (\ddot{x}_1 - \ddot{x}_i) \\
 z_1^b - z_i^b &= h_{32}^{-1} \cdot (\ddot{y}_1 - \ddot{y}_i) \\
 z_1^b - z_i^b &= h_{33}^{-1} \cdot (\ddot{z}_1 - \ddot{z}_i)
 \end{aligned} \tag{7}$$

For a given location on the vessel, Equation 7 shows that to estimate the x, y, and z components of a point's position relative to marker 1, a significant relationship is required with only the x, y, or z component of the point's relative acceleration. Once the coefficient h_{ij}^{-1} ($i = 1, 2, 3$ and $j = 1, 2, 3$) is known, using Equation 7, the difference in acceleration between two points can be used to compute the relative displacement between the two points.

IV. RESULTS AND DISCUSSION

The data from Run 1 (head seas, 0.06 m, 0.50 Hz) is used to illustrate how \mathbf{H}^{-1} was found and the centre of flotation was computed starting with the raw unfiltered acceleration measurement at points 1, 2, 3, 4 and 5 (Figure 6).

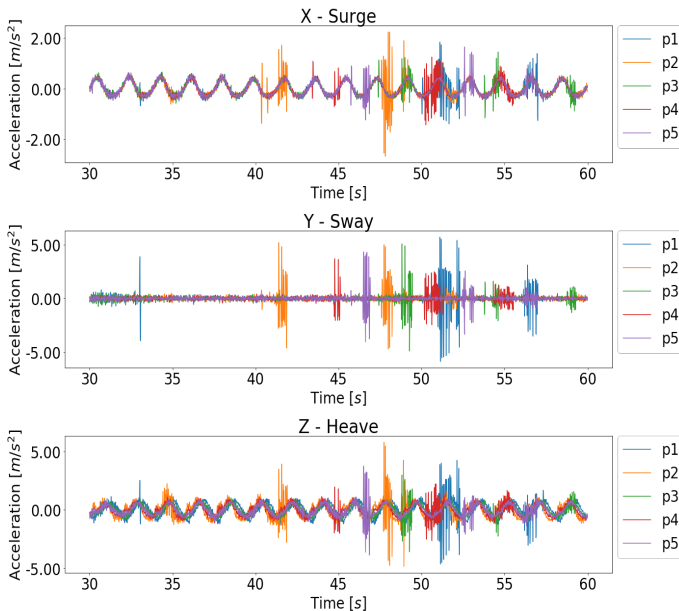


Fig. 6: Raw unfiltered acceleration measurements of markers 1, 2, 3, 4 and 5.

Figure 6 shows that there was high-frequency noise in the acceleration measurements. A high-order low-pass Butterworth filter was used to reduce the noise and remove outliers [41]. After filtering, the noise was reduced as seen in Figure 7. As seen in Equation 5, the method for estimating the centre of rotation of the ASV using only accelerometer measurements involves considering the difference between acceleration measurements at different positions on the ASV.

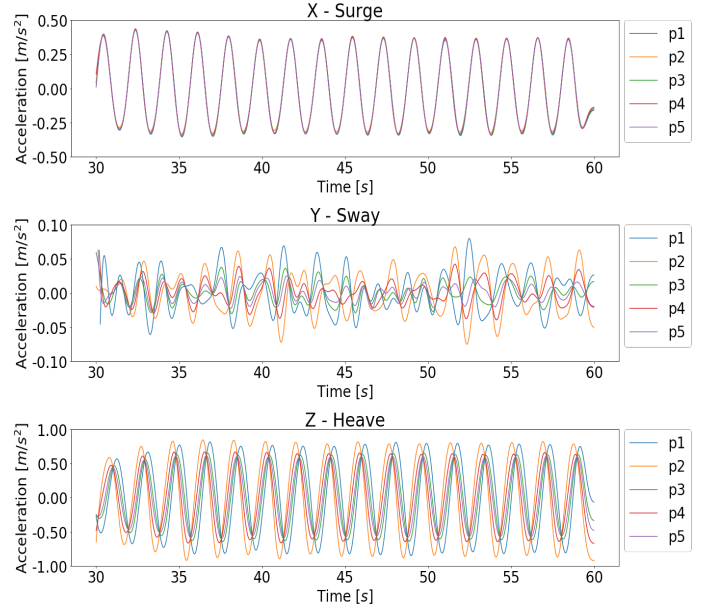


Fig. 7: Acceleration measurement of markers 1, 2, 3, 4 and 5 after filtering.

The filtered acceleration measurements for all markers were subtracted from the measurements from marker 1 to obtain data corresponding with Equation 5 (Figure 8).

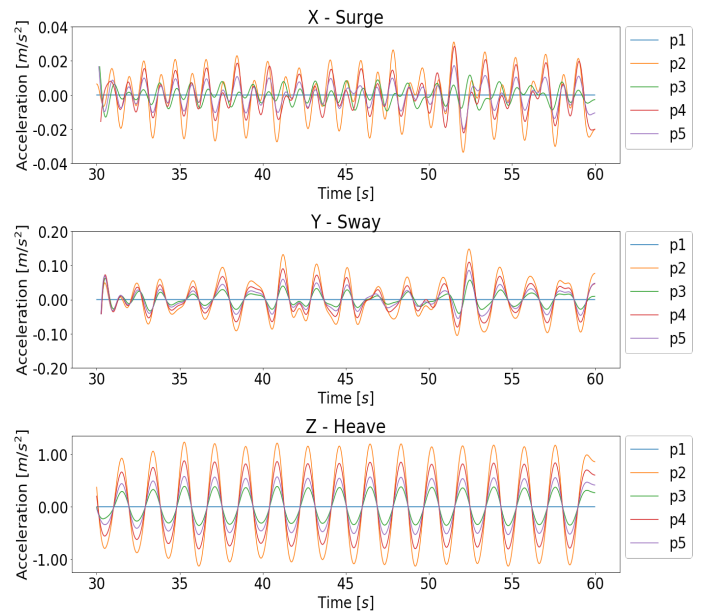


Fig. 8: Acceleration measurements for all markers relative to accelerations at marker 1.

In Figure 8, as expected the relative accelerations at point 1 were 0. Figure 8 shows that at certain moments in time, all the positions had the same acceleration measurements (relative acceleration = 0). To ensure that the data used in estimating the centre of flotation included only times when there was sufficient rotational motion, a peak finding algorithm [42] was used to find peaks in the relative acceleration measurements. Data was selected to include only the times at which the peaks occurred since we only wanted measurements at times when the acceleration measurements were different due to rotational motion. In the z component of the computed relative accelerations, the peaks corresponded to when the ASV was at its maximum pitch angle upwards and the troughs corresponded to the maximum pitch angle downwards.

The peak identification algorithm can be utilised on the data from any of the markers as the peaks occurred at the same time in all the marker positions. Figure 9 shows the peaks identified in the data from marker 2 in Run 1.

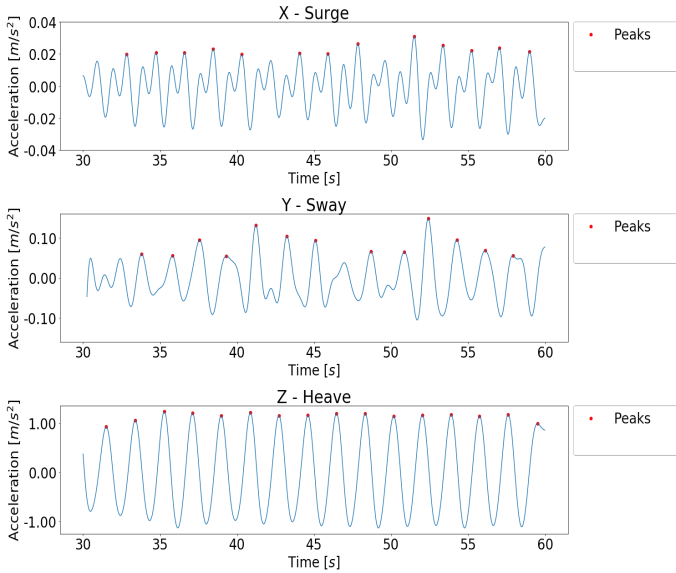


Fig. 9: Peak detection - Marker 2 relative acceleration measurements.

Figure 9 shows that the largest values of relative acceleration were in the z-axis. The identified peaks, when the ASV was at its maximum pitch angles, were used to estimate the location of the centre of flotation by using the set of simple regression equations shown in Equation 7 to compute the coefficient values in \mathbf{H}^{-1} . The coefficient values in \mathbf{H}^{-1} obtained from the regression are presented in Table IV.

In Table IV, the adjusted r-squared column shows how well the regression approximated the real data and was used together with the t-value to select which values in \mathbf{H}^{-1} were used in estimating the centre of rotation. These values were also useful for statistically evaluating the solution. The results reflected conclusions in earlier studies showing that when using Equation 3 to estimate the centre of flotation, angular motion is required. Since the vessel was in head waves, there was very little roll and yaw angular motion. Pitch motion occurred about the y-axis and was the major source of angular motion, resulting in all h_{ij}^{-1} values found involving the y

TABLE IV: Summary of regression results.

(a) Coefficients and standard error values

| Dependent | H | Independent | Coefficient | Standard Error |
|-----------------|---------------|---------------------------|-------------|----------------|
| $x_1^b - x_i^b$ | h_{11}^{-1} | $\ddot{x}_1 - \ddot{x}_i$ | -93.7342 | 3.515 |
| | h_{12}^{-1} | $\ddot{y}_1 - \ddot{y}_i$ | -23.3992 | 1.218 |
| | h_{13}^{-1} | $\ddot{z}_1 - \ddot{z}_i$ | -1.9340 | 0.017 |
| $y_1^b - y_i^b$ | h_{21}^{-1} | $\ddot{x}_1 - \ddot{x}_i$ | -7.7533 | 0.604 |
| | h_{22}^{-1} | $\ddot{y}_1 - \ddot{y}_i$ | -1.8936 | 0.211 |
| | h_{23}^{-1} | $\ddot{z}_1 - \ddot{z}_i$ | -0.1430 | 0.014 |
| $z_1^b - z_i^b$ | h_{31}^{-1} | $\ddot{x}_1 - \ddot{x}_i$ | 0.2081 | 0.090 |
| | h_{32}^{-1} | $\ddot{y}_1 - \ddot{y}_i$ | -0.1665 | 0.053 |
| | h_{33}^{-1} | $\ddot{z}_1 - \ddot{z}_i$ | -0.0931 | 0.001 |

(b) T and adjusted r-squared values

| Dependent | H | Independent | t | Adjusted R-Squared |
|-----------------|---------------|---------------------------|----------|--------------------|
| $x_1^b - x_i^b$ | h_{11}^{-1} | $\ddot{x}_1 - \ddot{x}_i$ | -26.670 | 0.932 |
| | h_{12}^{-1} | $\ddot{y}_1 - \ddot{y}_i$ | -19.203 | 0.876 |
| | h_{13}^{-1} | $\ddot{z}_1 - \ddot{z}_i$ | -112.870 | 0.995 |
| $y_1^b - y_i^b$ | h_{21}^{-1} | $\ddot{x}_1 - \ddot{x}_i$ | -12.829 | 0.759 |
| | h_{22}^{-1} | $\ddot{y}_1 - \ddot{y}_i$ | -8.969 | 0.604 |
| | h_{23}^{-1} | $\ddot{z}_1 - \ddot{z}_i$ | -10.460 | 0.629 |
| $z_1^b - z_i^b$ | h_{31}^{-1} | $\ddot{x}_1 - \ddot{x}_i$ | 2.317 | 0.078 |
| | h_{32}^{-1} | $\ddot{y}_1 - \ddot{y}_i$ | -3.116 | 0.143 |
| | h_{33}^{-1} | $\ddot{z}_1 - \ddot{z}_i$ | -90.629 | 0.992 |

components of relative position being poor estimates. Since the regression results showed a poor relationship between all relative acceleration values and the y components of relative position for this experimental setup, only the x and z components of the relative position of the centre of flotation were estimated using h_{13}^{-1} and h_{33}^{-1} respectively as seen in Equation 8.

$$\begin{aligned} x_1^b - x_i^b &= h_{13}^{-1} \cdot (\ddot{z}_1 - \ddot{z}_i) \\ z_1^b - z_i^b &= h_{33}^{-1} \cdot (\ddot{z}_1 - \ddot{z}_i) \end{aligned} \quad (8)$$

In order to estimate the location of the centre of rotation, the acceleration measurements from marker 2 were used since this marker had the largest acceleration measurements. Assuming the centre of flotation was at a point, C, Equation 8 is rewritten as

$$\begin{aligned} x_2^b - x_C^b &= h_{13}^{-1} \cdot (\ddot{z}_2 - \ddot{z}_C) \\ z_2^b - z_C^b &= h_{33}^{-1} \cdot (\ddot{z}_2 - \ddot{z}_C) \end{aligned} \quad (9)$$

To calculate the position of the centre of flotation using Equation 9, we needed to know the acceleration at the centre of flotation. To achieve this the following points were considered about the vessel:

- The rotational motion at the centre of rotation was always zero.
- In the z-axis, the maximum and minimum acceleration readings at the centre of rotation occurred when all points on the ASV had the same acceleration.
- In the z-axis, the acceleration of the centre of rotation of the ASV was zero when the absolute relative acceleration between two locations on the ASV were at a maximum as shown in Figure 10.

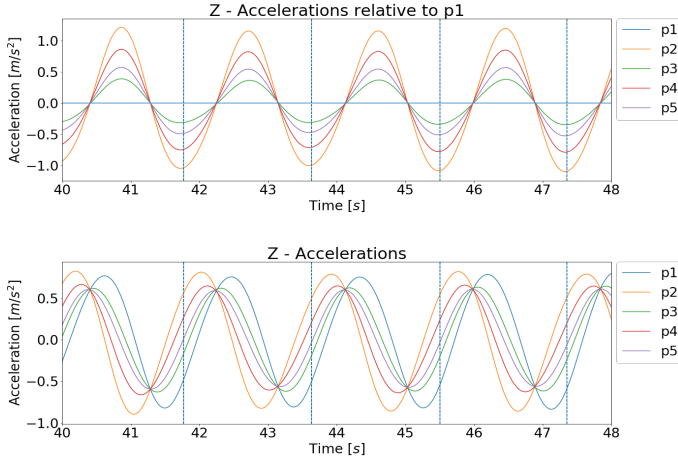


Fig. 10: Acceleration and relative acceleration measurements with times when the acceleration at the centre of flotation was zero (vertical dashed line)

Based on the stated points, we deduced that the times when the acceleration of the centre of rotation was temporarily zero coincided with when the peaks in relative acceleration occurred (the difference in acceleration measurements at two ends of the body were at a maximum).

Using the deduced times when the acceleration at the centre of flotation was zero and Equation 9, the average location of the centre of flotation when the ASV was at its minimum angle was calculated as 103.1 cm \pm 13.9 cm behind marker 2 in the x-axis and 4.0 cm \pm 0.6 cm below marker 2 in the z-axis. The

computed average location of the centre of flotation when the ASV was at its maximum angle was 126.8 cm \pm 10.7 cm behind marker 2 in the x-axis and 6.1 cm \pm 0.6 cm above marker 2 in the z-axis. The uncertainties associated with these values were calculated as the standard errors of prediction of the regression [43] and the uncertainties in the averages are calculated according to error propagation rules [44].

TABLE VI: Summary of the centre of flotation's position relative to marker 2 for each run.

(a) Head seas

| | At minimum pitch angle | | At maximum pitch angle | |
|------------|------------------------|----------------------|------------------------|----------------------|
| Run Number | $x_2^b - x_C^b$ [cm] | $z_2^b - z_C^b$ [cm] | $x_2^b - x_C^b$ [cm] | $z_2^b - z_C^b$ [cm] |
| 1 | 103.1 \pm 13.9 | -4.0 \pm 0.6 | 126.8 \pm 10.7 | 6.1 \pm 0.6 |
| 3 | 123.9 \pm 5.8 | -5.8 \pm 0.6 | 123.7 \pm 8.3 | 6.4 \pm 0.8 |
| 5 | 129.2 \pm 4.8 | -4.9 \pm 0.6 | 129.2 \pm 8.0 | 4.9 \pm 0.7 |
| 7 | 132.2 \pm 7.7 | -2.8 \pm 0.6 | 132.5 \pm 6.2 | 3.2 \pm 0.7 |
| Average | 122.1 \pm 4.4 | -4.4 \pm 0.3 | 128.1 \pm 4.2 | 5.2 \pm 0.4 |

(b) Following seas

| | At minimum pitch angle | | At maximum pitch angle | |
|------------|------------------------|----------------------|------------------------|----------------------|
| Run Number | $x_2^b - x_C^b$ [cm] | $z_2^b - z_C^b$ [cm] | $x_2^b - x_C^b$ [cm] | $z_2^b - z_C^b$ [cm] |
| 2 | 116.6 \pm 3.7 | -4.9 \pm 0.7 | 104.5 \pm 6.2 | 6.9 \pm 0.7 |
| 4 | 106.5 \pm 15.5 | -5.2 \pm 1.4 | 117.5 \pm 7.5 | 8.2 \pm 0.9 |
| 6 | 111.0 \pm 15.4 | -4.4 \pm 1.0 | 111.8 \pm 10.7 | 5.7 \pm 1.4 |
| 8 | 110.6 \pm 20.0 | -2.4 \pm 1.0 | 110.6 \pm 18.0 | 3.9 \pm 1.1 |
| Average | 111.2 \pm 7.5 | -4.2 \pm 0.5 | 111.1 \pm 5.8 | 6.2 \pm 0.5 |

TABLE V: Summary of pitch angles calculated using distance of centre of flotation from marker 2 assuming uncorrelated and random errors.

(a) Head seas

| | Minimum pitch angle of ASV[deg] | | Maximum pitch angle of ASV[deg] | |
|------------|---|---|---|---|
| Run Number | Computed from relative positions between marker 2 and centre of flotation | Calculated by optical motion capture system | Computed from relative positions between marker 2 and centre of flotation | Calculated by optical motion capture system |
| 1 | -2.222 \pm 0.008 | -2.220 \pm 0.050 | 2.754 \pm 0.006 | 2.734 \pm 0.050 |
| 3 | -2.680 \pm 0.005 | -2.455 \pm 0.050 | 2.962 \pm 0.007 | 3.226 \pm 0.050 |
| 5 | -2.172 \pm 0.005 | -1.689 \pm 0.050 | 2.172 \pm 0.006 | 2.658 \pm 0.050 |
| 7 | -1.213 \pm 0.005 | -0.859 \pm 0.050 | 1.383 \pm 0.005 | 1.670 \pm 0.050 |
| Average | -2.064 \pm 0.003 | -1.806 \pm 0.025 | 2.325 \pm 0.003 | 2.572 \pm 0.025 |

(b) Following seas

| | Minimum pitch angle of ASV[deg] | | Maximum pitch angle of ASV[deg] | |
|------------|---|---|---|---|
| Run Number | Computed from relative positions between marker 2 and centre of flotation | Calculated by optical motion capture system | Computed from relative positions between marker 2 and centre of flotation | Calculated by optical motion capture system |
| 2 | -2.406 \pm 0.006 | -2.970 \pm 0.050 | 3.778 \pm 0.008 | 3.209 \pm 0.050 |
| 4 | -2.795 \pm 0.015 | -3.465 \pm 0.050 | 3.992 \pm 0.009 | 3.465 \pm 0.050 |
| 6 | -2.270 \pm 0.011 | -2.914 \pm 0.050 | 2.919 \pm 0.013 | 2.597 \pm 0.050 |
| 8 | -1.243 \pm 0.010 | -1.825 \pm 0.050 | 2.020 \pm 0.011 | 1.617 \pm 0.050 |
| Average | -2.163 \pm 0.005 | -2.794 \pm 0.025 | 3.194 \pm 0.005 | 2.722 \pm 0.025 |

Table VI shows the estimated location of the centre of flotation during the eight runs at the maximum and minimum pitch angles. The variations within the uncertainties between the runs were affected by the goodness of fit of the regression to the data in each run. This varied depending on factors including the number of peaks identified, and the range of relative accelerations and positions.

For this experimental setup, the vertical position of the centre of mass was not determined because this does not affect the vessel's longitudinal stability aspect of trim. Considering the centre of mass was 129 cm behind marker 2, the results in Table VI show that on average the centre of flotation was further behind marker 2 and closer to the centre of mass of the ASV in head seas compared to following seas. In Run 7 and Run 8 the z component of the relative position was comparatively low due to the ASV's wave encounter frequency. This reduction in distance was due to a relatively smaller pitch angle as the encounter frequency increased with the wave amplitude remaining constant.

The results were given with respect to a marker rather than the centre of mass because during a vessel's operation at sea, the centre of mass changes as weights change on board. On the contrary, the locations of acceleration measurements on a vessel remain fixed and serve as an appropriate reference point. These results were validated by using the computed displacement between the centre of flotation and marker 2 to calculate the ASV pitch angle using Equation 10.

$$\theta = \tan^{-1} \left(\frac{z_2^b - z_C^b}{x_2^b - x_C^b} \right) \quad (10)$$

The errors associated with the distances, $z_2^b - z_C^b$ and $x_2^b - x_C^b$, were assumed to be uncorrelated and random [44]. These values were compared with the angles measured by the optical motion capture system as shown in Table V. In head seas, the minimum pitch angles from the optical motion capture system were lower than the computed angles and the maximum pitch angles from the optical motion capture system were higher than computed. The opposite was observed in following seas. Upon examination of the experimental setup this was found to be due to a systematic error from the L-frame, which determined the optical motion capture system's reference frame. The L-frame was not absolutely parallel to the still water surface. With the L-frame angled slightly upwards (less than 1 degree) towards the wavemaker, Qualisys overestimated the upwards pitch when the ASV was heading towards the wavemaker and underestimated the downwards pitch. This was opposite when the ASV was heading away from the wavemaker; the upwards pitch was underestimated and the downwards pitch was overestimated.

The results are comparable and show that the absolute value of the maximum pitch was usually greater than the absolute value of the minimum pitch. This is expected due to the longitudinal asymmetry of the hull causing a difference in the submerged volume when the vessel pitches positively and negatively [45].

V. CONCLUSION AND FUTURE WORK

This paper presented a novel technique for estimating the longitudinal centre of flotation of a vessel in waves. The proposed method was based on acceleration measurements along the length of the vessel. Table IV showed the importance of sufficient angular motion to robust estimation of the location of the centre of rotation. Additional markers can be used to improve the precision of the proposed method for computing the location of the centre of flotation.

The proposed solution presented has many potential applications since knowledge of the position of the centre of flotation is essential for ensuring proper distribution of weights on a vessel and stability. Compared to approaches for vessels not in waves which assume the centre of flotation is fixed, the proposed method does not require knowledge of positions and quantities of weights on board a vessel. This solution can also be developed to assess a vessel's static stability by estimating its metacentric height, similar to previous work applying smartphones to ship stability experiments [46].

A similar experimental setup with roll motion rather than pitch motion can be used to estimate the transverse location of the centre of flotation. The acceleration measurements recorded using the optical motion capture system can also be compared with measurements from low-cost off-the-shelf accelerometers. This will enable the presented method to be used at sea with a network of accelerometers without requiring a shore-based setup.

ACKNOWLEDGMENT

The authors would like to thank Bertrand Malas, the towing tank manager, for all his guidance during the data collection process. This project is funded by the Engineering and Physical Sciences Research Council (EPSRC reference number 1368760). The dataset used in this paper is available at <https://doi.org/10.5258/SOTON/D0534>.

REFERENCES

- [1] R. Poku, T. W. Oyink, C. A. N. Johnson, and E. A. Ogbonnaya, "The effects of weight changes on ships stability," *British Journal of Applied Science and Technology*, vol. 16, no. 1, pp. 1 – 9, 2016.
- [2] P. Krata, "The impact of sloshing liquids on ship stability for various dimensions of partly filled tanks," *The International Journal on Marine Navigation and Safety of Sea Transportation*, vol. 7, no. 4, pp. 481 – 489, 2013.
- [3] K. J. Rawson and E. C. Tupper, *Basic Ship Theory*, 5th ed. Butterworth-Heinemann, 2001.
- [4] H. J. Pursey, *Merchant Ship Stability*, 6th ed. Brown, Son & Ferguson, 1996.
- [5] J. Kliava and J. M  gel, "Non-uniqueness of the point of application of the buoyancy force," *European Journal of Physics*, vol. 31, no. 4, p. 741, 2010.
- [6] J. M  gel and J. Kliava, "Metacenter and ship stability," *American Journal of Physics*, vol. 78, no. 7, pp. 19–21, 2010.
- [7] D. Paroka and N. Umeda, "Effect of freeboard and metacentric height on capsizing probability of purse seiners in irregular beam seas," *Journal of Marine Science and Technology*, vol. 12, no. 3, pp. 150 – 159, 2017.
- [8] J. L. Herder and A. L. Schwab, "On dynamically equivalent force systems and their application to the balancing of a broom or the stability of a shoe box," in *Proceedings of DETC04 ASME Design Engineering Technical Conferences and Computers and Information in Engineering Conference*, New York, USA, 2004.
- [9] C. Dupin, *Applications de g  om  trie de m  canique    la marine, aux ponts et chauss  es; pour faire suite aux d  veloppemens de g  om  trie*, Paris, 1822.

- [10] P. Bouguer, *Traité du Navire, de sa construction, et de ses mouvemens*, Paris, 1746.
- [11] H. Nowacki and L. D. Ferreira, *Historical Roots of the Theory of Hydrostatic Stability of Ships*. Dordrecht: Springer Netherlands, 2011, pp. 141–180.
- [12] A. Jain and V. Kanhangad, “Human activity classification in smartphones using accelerometer and gyroscope sensors,” *IEEE Sensors Journal*, vol. 18, no. 3, pp. 1169–1177, Feb 2018.
- [13] A. Sabato, C. Niezrecki, and G. Fortino, “Wireless mems-based accelerometer sensor boards for structural vibration monitoring: A review,” *IEEE Sensors Journal*, vol. 17, no. 2, pp. 226–235, Jan 2017.
- [14] M. Ghanbari and M. J. Yazdanpanah, “Delay compensation of tilt sensors based on mems accelerometer using data fusion technique,” *IEEE Sensors Journal*, vol. 15, no. 3, pp. 1959–1966, March 2015.
- [15] Y. M. Al-Rawashdeh, M. Elshafei, and M. F. Al-Malki, “In-flight estimation of center of gravity position using all-accelerometers,” *Sensors*, vol. 14, no. 9, pp. 17567–17585, 2014.
- [16] Z. Jun, H. He, and L. Yingying, “Spacecraft center of mass online estimation based on multi-accelerometers,” in *2nd IEEE International Conference on Information Management and Engineering*, Chengdu, 2010, pp. 295–298.
- [17] J. E. Marsden and T. S. Ratiui, *An Introduction to Mechanics and Symmetry: A Basic Exposition of Classical Mechanical Systems*, 2nd ed. Springer, 1999.
- [18] Hapag-Lloyd, “How vessel trim optimisation creates efficiencies,” 2018, [Online; accessed 27 June 2018] <https://www.hapag-lloyd.com/en/news-insights/insights/2017/03/how-vessel-trim-optimisation-creates-efficiencies.html>.
- [19] K. H. Su, “Anti-rolling fin control for ship stabilization,” in *2013 CACS International Automatic Control Conference (CACS)*, Dec 2013, pp. 389–394.
- [20] A. Benetazzo, “Accurate measurement of six degree of freedom small-scale ship motion through analysis of one camera images,” *Ocean Engineering*, vol. 38, no. 16, pp. 1755 – 1762, 2011.
- [21] E. Nocerino, F. Menna, and F. Remondino, “Comparison between single and multi-camera view videogrammetry for estimating 6dof of a rigid body,” in *Proc.SPIE, Videometrics, Range Imaging, and Applications XIII*, vol. 9528, Munich, Germany, 21 June 2015.
- [22] S. Bennett, C. Brooks, B. Winden, D. Taunton, A. Forrester, S. Turnock, and D. Hudson, “Measurement of ship hydroelastic response using multiple wireless sensor nodes,” *Ocean Engineering*, vol. 79, pp. 67 – 80, 2014.
- [23] N. O. Abankwa, S. J. Johnston, M. Scott, and S. J. Cox, “Ship motion measurement using an inertial measurement unit,” in *2015 IEEE 2nd World Forum on Internet of Things (WF-IoT)*, Milan, Italy, 14 - 16 Dec 2015, pp. 375–380.
- [24] N. O. Abankwa, G. Squicciarini, S. J. Johnston, M. Scott, and S. J. Cox, “An evaluation of the use of low-cost accelerometers in assessing fishing vessel stability through period of heave motion,” in *2016 International Conference for Students on Applied Engineering (ICSAE)*, Newcastle upon Tyne, UK, 20 - 21 Oct 2016, pp. 59–63.
- [25] M. Wolf, G. Liebsch, A. Richter, and R. Dietrich, “Marine motion measurements using gps,” *International Hydrographic Review*, vol. 4, no. 3, pp. 6–21, 2003.
- [26] J. M. Nunez, M. G. Araujo, and I. Garcia-Tunon, “Real-time telemetry system for monitoring motion of ships based on inertial sensors,” *Sensors*, vol. 17, no. 5, pp. 948–969, 2017.
- [27] Wolfson Unit, “Model Basins,” 2016, [Online; accessed 9 April 2018] <http://www.wumtia.soton.ac.uk/facilities/model-basins>.
- [28] J. Bowker, N. Townsend, M.-Y. Tan, and A. Shenoi, “Experimental analysis of submerged flapping foils; implications for autonomous surface vehicles (asvs),” in *OCEANS 2016 MTS/IEEE Monterey*. IEEE, December 2016.
- [29] Qualisys Motion Capture Systems, “Oqus Cameras,” 2018, [Online; accessed 27 June 2018] <https://www.qualisys.com/cameras/okus/#tech-specs>.
- [30] —, “Qualisys Mocap System Summary and Purchasing information,” 2016, [Online; accessed 9 April 2018] <http://teachers.d11.org/teachers/wybrasr/Shared%20Documents/FlightGrantQuotes/QualisysInfo.pdf>.
- [31] O. Faugeras, *Three-Dimensional Computer Vision: A Geometric Viewpoint*. MIT Press, 1994.
- [32] K.-Y. Shin and J. H. Mun, “A multi-camera calibration method using a 3-axis frame and wand,” *International Journal of Precision Engineering and Manufacturing*, vol. 13, no. 2, pp. 283–289, Feb 2012.
- [33] N. A. Borghese and P. Cerveri, “Calibrating a video camera pair with a rigid bar,” *Pattern Recognition*, vol. 33, no. 1, pp. 81 – 95, 2000.
- [34] E. Schoonderwaldt and D. Thompson, “Learn about 6DOF,” 2016, [Online; accessed 27 June 2018] <https://www.qualisys.com/webinars/learn-about-6dof/>.
- [35] J. R. Taylor, *Classical Mechanics*. University Science Books, 1997.
- [36] S. T. Thornton and J. B. Marion, *Classical dynamics of particles and systems*, 5th ed. Brooks and Cole, 2004.
- [37] S. Liu and G. Trenkler, “Hadamard, khatri-rao, kronecker and other matrix products,” *International Journal of Information and Systems Sciences*, vol. 4, no. 1, pp. 160–177, 2008.
- [38] J. D. Hamilton, *Time Series Analysis*. Princeton University Press, 1994.
- [39] J. Hartikainen and S. Sarkka, “Kalman filtering and smoothing solutions to temporal gaussian process regression models,” in *2010 IEEE International Workshop on Machine Learning for Signal Processing*, Aug 2010, pp. 379–384.
- [40] S. J. Koopman, “Exact initial kalman filtering and smoothing for nonstationary time series models,” *Journal of the American Statistical Association*, vol. 92, no. 440, pp. 1630–1638, 1997.
- [41] S. Butterworth, “On the theory of filter amplifiers,” *Experimental wireless and the wireless engineer*, vol. 7, pp. 536–541, 1930.
- [42] L. H. Negri, “PeakUtils,” 2016, [Online; accessed 11 April 2018] <https://pypi.python.org/pypi/PeakUtils>.
- [43] B. Larget, “Estimation and Prediction,” 2007, [Online; accessed 20 May 2018] <http://www.stat.wisc.edu/courses/st572-larget/Spring2007/handouts03-1.pdf>.
- [44] J. R. Taylor, *An Introduction to Error Analysis*. University Science Books, 2005.
- [45] P. Ghadimi, A. Dashtimanesh, S. R. Djeddi, and Y. F. Maghrebi, “Development of a mathematical model for simultaneous heave, pitch and roll motions of planing vessel in regular waves,” *International Journal of Scientific World*, vol. 1, no. 2, pp. 44–56, 2013.
- [46] A. Djebli, B. Hamoudi, O. Imine, and L. Adjilout, “The application of smartphone in ship stability experiment,” *Journal of Marine Science and Application*, vol. 14, pp. 406–412, 10 2015.



Nana O Abankwa is a Postgraduate research student in the Computational Engineering and Design Research Group within the Faculty of Engineering and the Environment. Prior to this, he obtained a first-class degree in Mechanical Engineering at the University of Southampton. Nana has won a number of competitions including being part of the team that came 1st place in the micro-sailboat class of the 2016 World Robotic Sailing Championship and winning the 2017-2018 Rolls-Royce Data Storytelling Challenge. His research project focuses on methods

of acquiring data related to vessel safety using IoT devices. His other interests include data visualisation and machine learning.



James Bowker is a Postgraduate research student within Engineering and the Environment at the University of Southampton. James received a Master of Engineering (M.Eng.) degree in Ship Science/Naval Engineering from the University of Southampton. His research projects are on wave energy scavenging for autonomous marine systems and energy harvesting utilizing the gyroscopic effect. His research interests include marine renewable energy / sustainable energy systems, seakeeping, bioinspiration / biomimicry and marine robotics.



Steven J Johnston is a Senior Research Fellow in Engineering and the Environment at the University of Southampton. Steven completed a Ph.D. with the Computational Engineering and Design Group (CED) and he also received an M.Eng. degree in Software Engineering from the School of Electronics and Computer Science (ECS). Steven has participated in 40+ outreach and public engagement events as an outreach program manager for Microsoft Research. He currently operates the LoRaWAN wireless network for Southampton and

his current research includes the large-scale deployment of environmental sensors. He is a member of IET.



Simon J Cox is Professor of Computational Methods and Chief Information Officer at the University of Southampton. He has a doctorate in Electronics and Computer Science, first-class degrees in Maths and Physics and has won over 30M in research & enterprise funding, and industrial sponsorship. He has published over 250 papers. He has co-founded two spin-out companies and, as Associate Dean for Enterprise, has most recently been responsible for a team of 100 staff with a 11M per year turnover providing industrial engineering consultancy, large-

scale experimental facilities and healthcare services.



Mark Scott joined the University of Southampton in 2001 as an IT Systems Architect and Developer. After working for several groups in the School of Engineering Sciences, he moved to the central IT Department and completed a PhD on the management of materials engineering and medical research data, and now leads one of its innovation teams. He is interested in the use of IoT devices in research laboratories, including the management and curation of the data and metadata produced. Other interests include data visualisation, machine learning, and

augmented and virtual reality.